Macromolecular Materials and Engineering
www.mme-journal.de

Fiber-Optic Photoacoustic Generator Realized by Inkjet-Printing of CNT-PDMS Composites on Fiber End Faces

Patrick Oser, Johannes Jehn, Michael Kaiser, Oliver Düttmann, Fabian Schmid, Levin Schulte-Spechtel, Sergio Sánchez Rivas, Constanze Eulenkamp, Christina Schindler,* Christian U. Grosse,* and Datong Wu**

In recent years, photoacoustic generators based on multiwalled carbon nanotubes (MWCNT) and polydimethylsiloxane (PDMS) are manufactured in a variety of ways, which influences the properties of the generators with respect to frequency bandwidth, sound wave pressure, robustness, and reproducibility. Due to the high optical absorption of MWCNTs and the high thermal expansion coefficient of PDMS, this combination is ideally suited for use as a photoacoustic generator. This study presents a novel method to produce photoacoustic generators based on long-term stable MWCNT and PDMS inks with a high reproducibility by means of inkjet-printing. The MWCNT-PDMS layers (thicknesses of 2–4 µm), printed directly onto the distal end face of a multimode glass fiber, show a good homogeneity and low optical transmission (19–21%). After the preparation of the fiber pieces, the inkjet printer performs all steps automatically in a time period of 30–60 s per layer. The generated ultrasonic pressure (0.39–0.54 MPa) and frequency bandwidth (1.5–12.7 MHz) can be measured at a distance of ≈4 mm with a laser fluency of 12.7 mJ cm^{-2}. These highly reproducible printed photoacoustic generators can be well used for nondestructive material testing and medical applications.

1. Introduction

For many years research in photoacoustic generators has offered far-reaching possibilities in nondestructive materials testing and in medical imaging applications.[1–8] Photoacoustic applications have some limitations on sensitive materials such as on living tissues, since the risk of burns or ablation due to excessive heat deposition limits the amount of used laser energy. For applications on such kind of sensitive materials, the approach with a highly optical absorbing intermediate layer becomes more interesting,[7,9,10] where a sample is not directly illuminated by a laser beam but instead a robust, optical absorbing coating layer can be applied for ultrasound generation. These intermediate layers work as a complementary method for classical photoacoustics, which provide molecular contrast for ultrasonic imaging. Due to the high degree of optical absorption,[11] these thin layers can absorb more laser energy and therefore generate higher ultrasound pressures without damaging samples or tissues. The design of these layers ranges from pure nanoparticle coatings to pure metal layers,[5,12–17] the mixed combination of nanoparticles, and polymers.[6,11,18,19] For the purpose of high optical absorption gold nanostructures,[20–22] graphite,[6,23] carbon fibers,[24,25] carbon black,[18,26] and candle soot[4,27–29] have been investigated. One kind of nanoparticles is clearly outstanding for these applications[19,30,31] due to its extreme high and broadband optical absorption:[32–35] carbon nanotubes. The efficiency for ultrasound generation can be improved by an additional elastomer component such as polydimethylsiloxane (PDMS), since PDMS has a high volumetric coefficient of thermal expansion of $\beta = 300 \times 10^{-6}$ C^{-1}[36–38] and at the same time low optical absorption.[39–41] However, the production methods depending on the manufacturing process can vary significantly (**Table 1**), which have strong impacts on coating parameters such as layer thicknesses, degree of transmission and ultrasound pressures, as well as frequency bandwidths. Common production methods of these coatings are blade-coating,[22] dip-coating,[2,10,19,42] or spin-coating, sometimes in combination with chemical vapor deposition (CVD),[38,43] vacuum filtration,[37] or electrospinning[11] as well as spray-coating.[41]

The drop-on-demand (DOD) procedure with inkjet-printing allows a precise production of desired structures[48–53] without the need for expensive masks[54] as used in screen-printing[55–59] or other post-treatments such as etching, mechanical scratching, or processing methods in baths.[60,61] Inkjet-printing is already successfully used in printed electronics for temperature[62–64] or

P. Oser, J. Jehn, M. Kaiser, O. Düttmann, F. Schmid, L. Schulte-Spechtel, S. S. Rivas, Dr. C. Eulenkamp, Prof. C. Schindler, Prof. D. Wu
Department of Applied Sciences and Mechatronics
University of Applied Sciences Munich
Lothstraße 34, Munich 80335, Germany
E-mail: patrick.oser@hm.edu; christina.schindler@hm.edu; datong.wu@hm.edu
Prof. C. U. Grosse
Department of Civil Geo and Environmental Engineering
Chair of Non-Destructive Testing
Technical University of Munich
Baumbachstr. 7, Munich 81245, Germany
E-mail: grosse@tum.de
The ORCID identification number(s) for the author(s) of this article can be found under https://doi.org/10.1002/mame.202000563.

DOI: 10.1002/mame.202000563

Table 1. Comparison and characterization of the current manufactured multiwalled carbon nanotubes (MWCNT) with polydimethylsiloxane (PDMS) for photoacoustic transducers regarding design, generated sound pressure, frequency bandwidth, and layer thickness, as well as the used lasers. The table is taken from previous work. Adapted with permission under the terms of the Creative Commons Attribution-NonCommercial-NoDerivs License.[41] Copyright 2020, the Authors. Published by Wiley-VCH GmbH.

Design Nanoparticle, polymer	Coating method Processing time [h]	Layer thickness [µm] Bandwidth [MHz] Sound pressure [MPa]	Pulse duration [ns] Wavelength [µm] Fluency [mJ cm^{-2}]	Reference
300 µm fiber, MWCNT, PDMS	Dip-coating 24+	20 26.5 ≈4	2 1064 ≈36	M. C. Finlay[a)]
200 µm fiber, MWCNT, PDMS	Dip-coating 24+	20, 20 15, 20 4.5, 4	2, 2 1064, 1064 36.6, 96	R. J. Colchester[b)]
200 µm fiber, MWCNT, PDMS	Dip-coating 24+	20 ≈40 4.5	2 1064 36.1	S. Noimark[c)]
Epoxy slab distal end of a 400 µm fiber, MWCNT, PDMS	Dip-coating 24+	– 31.3 1.87	2 1064 8	R. J. Colchester[b)]
Membrane, MWCNT, PDMS	Blade-coating 24+	46 27.2 ≈1	5 1064 76 µJ pulse^{-1}	E. J. Alles[d)]
200 µm fiber, MWCNT, PDMS	Electrospinning, PDMS dip-coating 48+	13.7 29 1.59	2 1064 35	R. K. Poduval[e)]
Glass slab, MWCNT, PDMS	CVD, spin-coating Few hours	2.6 80 –	3 532 43.4	H. W. Baac[f)]
Coated PMMA film, MWCNT, PDMS	Vacuum filtration/transition, spin-coating 16+	9 10 6.35	8 532 180 mW pulse^{-1}	X. Fan[g)]
PET slab, MWCNT, PDMS	Vacuum filtration/transition, spin-coating 16+	20 10 5.4	8 532 330 mJ pulse^{-1}	X. Fan[g)]
PET lens, MWCNT, PDMS	Vacuum filtration/transition, spin-coating 16+	20 10 35	8 532 330 mJ pulse^{-1}	X. Fan[g)]
PMMA substrate, MWCNT, PDMS	Vacuum filtration method, spin-coating n.a.	5.2 15 3.2	8 532 180 mW cm^{-2}	C. Moon[h)]
Coated lens, MWCNT, gold, PDMS	CVD, gold deposition, spin-coating Few hours	2.6 30 57	6 532 42.4	H. W. Baac[i)]
Coated lens, MWCNT, gold, PDMS	CVD, gold deposition, spin-coating Few hours	16 25 70	6 532 9.6	T. Lee[i)]
Coated glass slab, MWCNT, PDMS	Spray coating >2	0.9–32 9.7 3.4	11.4 1047 17.2	P. Oseri[j)]

Values were taken from: [a)]Ref. [10]; [b)]Refs. [2, 19, 42]; [c)]Ref. [44]; [d)]Ref. [22]; [e)]Ref. [45]; [f)]Ref. [30]; [g)]Ref. [46, 47]; [h)]Ref. [37]; [i)]Ref. [38, 43]; [j)]Ref. [41].
Note: Processing time: processing of the nanoparticles into a solution, application to the sample, and finalization of the photoacoustic generator (application of the polymer, curing). The curing time varies greatly with temperature (48 h at 25 °C and 10 min at 150 °C) and is not in the table.

strain/stress sensor,[62,65,66] and is therefore suitable to produce fully inkjet-printed photoacoustic generators. Compared to the methods in Table 1, the DOD procedure offers a suitable extension to produce thin photoacoustic generators.

In this study, we present a novel method to produce a fully inkjet-printed photoacoustic generator. The characterization of this method includes the investigation of the self-made long-term stable inks, evaluation of printing homogeneity, and the determination of the photoacoustic performances. The manufacturing process was performed exclusively with a Dimatix Materials Printer DMP-2831. The photoacoustic actuators were printed on the distal end face of multimode short fiber

sections, which were coupled afterward with a fiber extension for ultrasonic investigations. The developed manufacturing process of these CNT/PDMS coatings is easy to handle, reproducible, robust, and independent of the use of potentially toxic chemicals as solvents. The shape and number of the fully inkjet-printed layers can be controlled, which results in a reduction of production time, less costs, and reduced waste for thin layers. The method presented in this study enables a precise and reproducible production of thin but sufficiently highly optical absorbent layers for ultrasonic actuators in which all printing process steps (except ink production, cartridge exchange, and substrate handling) are performed automatically. Due to a suitable frequency bandwidth and pressure level, the printed photoacoustic generators can be well used in the field of nondestructive testing of layered materials or in medicine.

2. Experimental Section

2.1. Materials

Multiwalled carbon nanotubes (MWCNTs) provided by Sigma Aldrich (724769-100G) were produced by CVD using cobalt and molybdenum as catalysts (CoMoCAT). The outer diameters of the MWCNTs (95% carbon) are 6–9 nm and lengths around 5 µm, respectively. Polyoxyethylene octyl phenyl ether (Triton-X-100) is a *p*-tertoctylphenol derivative with a polyethylene glycol side chain of 9–10 ethylene oxide units. It is a nonionic surfactant from the group of octylphenol ethoxylates. Sylgard 184 was provided by Dow Corning and consists of PDMS and a curing agent (CA). Octamethyltrisiloxane (poly(dimethylsiloxane), 469319) was provided by Sigma Aldrich. All chemicals were used as delivered, and no further changes were made.

2.2. Ink Production and Inkjet-Printing

For printing photoacoustic transducers, a water-based CNT-PDMS ink on the basis of Triton-X-100 and a polymer-based PDMS CA ink were prepared. Triton-X-100 is well suited for dissolving CNTs[67–71] in water. In addition, it is also suitable for dissolving PDMS in a water-based solution, making Triton-X-100 an excellent mediator between CNTs and PDMS in a water-based solution, which results in a nontoxic CNT-PDMS ink. The manufacturing process and analysis of the PDMS-CNT-ink was described in a previous work, and was done in under 2 h.[41] The PDMS curing agent (PDMS-CA) ink is based on a hydrophobic short-chain PDMS with a low viscosity of 1 cSt at 25 °C as a solvent, since PDMS dissolves very well in other PDMS types.[72] The PDMS-CA ink was prepared using a short-chain and viscous octamethyltrisiloxane solution. The undissolved components in the solution were homogenized for 2 min by using a 130 W ultrasonic homogenizer. The highly homogenized short polymer PDMS solution was very stable for the application and could still be used after more than half a year without changing its properties. For this purpose, the inks (CNT-PDMS and PDMS-CA) were stored in a refrigerator at 0 °C and periodically examined whether properties such as curing time, shape, speed, and direction of the ejected drops, and direction, or printability change with time. These tests were carried out over a period of half a year. As with the CNT ink, refilling the printer cartridges was possible, which results in a significant reduction of waste and used materials. For the printing tests, the self-developed inks were taken out of the refrigerator, the required amount was filled into the printer cartridge, and then stored again in the refrigerator at about 0 °C. A significant improvement of ink stability compared to previous works can be achieved, which reported a stability of PDMS inks of 2 h[73] and most recently a stability of 2 d.[74] The curing time of these inks does not exceed that of untreated PDMS.

The inkjet-printing of CNT-PDMS photoacoustic generators was performed by using the Dimatix Materials Printer DMP-2831 with a cartridge with a drop volume of 10 pL and a nozzle with a diameter of 21 µm at room temperature (20–25 °C). The nozzles were driven by a piezo element that allows the deposition of a single droplet by a voltage pulse. The built-in drop-watcher was used to monitor the properties like the speed of ejection, drop shape, and direction of the ink during printing. The voltage settings of the piezo-driven nozzles were optimized to maximize drop stability and minimize the formation of satellite drops. The shape, speed, and direction of the ejected drops were periodically checked with the built-in drop-watcher to determine whether the ink properties remained constant during printing processes.

The inkjet-printing was performed on 16–18 mm long, polished glass fiber end faces (1 mm diameter and 0.50 NA step index multimode fiber, Thorlabs FP1000URT) which were placed face up on the printing plate in a custom-made fiber holder (**Figure 1**). Prior to inkjet-printing, the fiber end faces were cleaned with 2-propanol.

In order to determine printing parameters for the best and most homogeneous CNT coatings, a series of tests with different line spacing was carried out before printing onto the fiber end faces (**Figure 2**).

The CNT-PDMS ink was best printed with a line spacing of 50–100 µm and a drop spacing of 10 µm based on a visual inspection. Afterward, the printed PDMS-CA ink had a line spacing

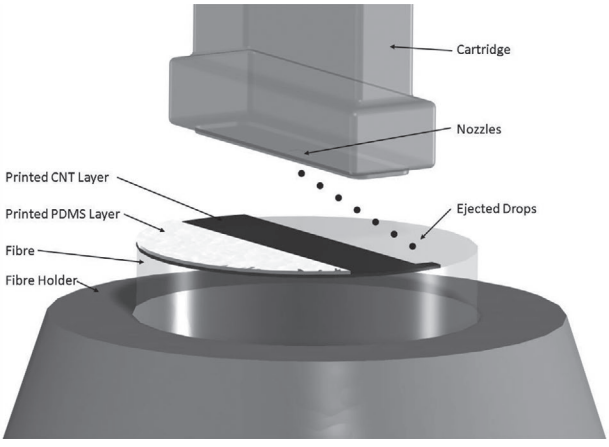

Figure 1. Schematic representation of the coating process using inkjet-printing. A custom-made fiber holder straightens the fiber (diameter 1 mm) vertically, while CNT-PDMS and PDMS-CA were sequentially printed onto the fiber end faces. The printing process took about 30–60 s per layer. The diameters of the cartridge nozzles are ≈21 µm.

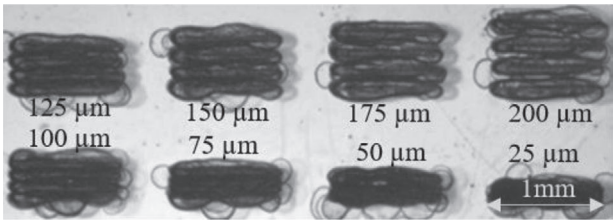

Figure 2. Investigation and determination of suitable line spacings for homogeneous coatings. Four 1 mm long lines were printed with a line spacing of 25 µm up to 200 µm. Line spacing was increased clockwise by 25 µm each, starting from 25 µm bottom right. The linewidth is around 200 µm for 20–40 layers.

Table 2. Overview of investigated printing parameters for printing the fiber samples.

	Fiber 1	Fiber 2	Fiber 3
MWCNT-PDMS layers	20	40	20
PDMS-CA layers	3	6	6
Line spacing [µm]	100	100	50
Printing time [min]	≈15	≈25	≈25

of 10 µm and a drop spacing of 10 µm, which showed the best inspection results. The printing parameters were varied except the drop spacing which remained at 10 µm (**Table 2**), in order to obtain the most homogeneous coating. The printing layout for a Ø 1 mm fiber had an area of 1.5 mm^2 to have some overlap for a homogeneous coating. With a line spacing of 50 µm the printing speed for one CNT ink nozzle was 0.05 $mm^2\ s^{-1}$ and with a line spacing of 100 µm the printing speed was 0.025 $mm^2\ s^{-1}$, respectively. The minimum print area depends on the number of layers and is limited primary by the drop dimension, which is about 50–200 µm in diameter. This results in a minimum line width of 50–200 µm depending on the number of layers. The maximum printable area is the area of the printing plate of the printer. The total printing process can take about 15–25 min, depending on the number of layers as well.

The homogeneity of coatings (**Figure 3**) as well as the coating thicknesses were determined with a scanning electron microscope (SEM-FIB LYRA from Tescan). A part of the coating was mechanically removed with a scalpel from the fiber end face. The layer thicknesses were between 2 and 4 µm (**Figure 4a**) and a fully inkjet-printed fiber tip is shown in Figure 4b.

The optical transmission coefficient of the fibers was determined by measuring the laser transmission power levels. As reference, a fiber of the same design and with the same number of couplings (**Figure 5**) but without any coating was used. Since both the coated fiber and the reference fiber were of the same design and had the same coupling loss of laser power, the power transmission ratio of these two measurements was taken into account in the absorption calculation. The coated fibers with coating thicknesses of 2–4 µm showed a reduction of the laser power of 79–81% in comparison to reference fiber values at a wavelength of 1047 nm. The optical absorption level (≈80%) is also consistent with other applications of very thin CNT films and undirected nonforest CNT layers.[19,30,31,44]

3. Assembling and Ultrasonic Characterization

Depending on the selected line spacing (**Table 2**), the printing process took 30–60 s per layer. After the printing process, the short fiber pieces were placed in an oven at 150 °C for 10 min in order to accelerate the curing process of the PDMS. After curing, the short fiber pieces were coupled with a fiber extension to make them suitable for the coupling system (BFT1 Universal Bare Fibre Terminator, Thorlabs). A Ceramic Split Mating Sleeve (ADAL1) of Ø 1.25 mm (LC/PC) from Thorlabs was used to connect the two fibers as shown in Figure 5. Finally, a shrink tubing was applied to hold the parts tightly in place.

The ultrasonic pressure in water was measured with a PVDF needle hydrophone (Imotec measuring technique: type 80-0.5-4.0, 1 mm diameter). The measurement setup was described and shown in our previous work.[41] A multimode fiber (1 mm diameter, 0.50 NA step index multimode for the laser excitation the FP1000URT fibre, Thorlabs) was used, which was coupled with a fiber collimator (RC08FC-F01: reflector collimator, UV amplified, Ø 8.5 mm beam, FC/PC). The used laser was a Q-switched laser (Mosquito Innolas, Germany) with a wavelength of 1047 nm, a pulse duration of 11.4 ns, and a repetition rate of 1 kHz. The laser power was about 100 mW

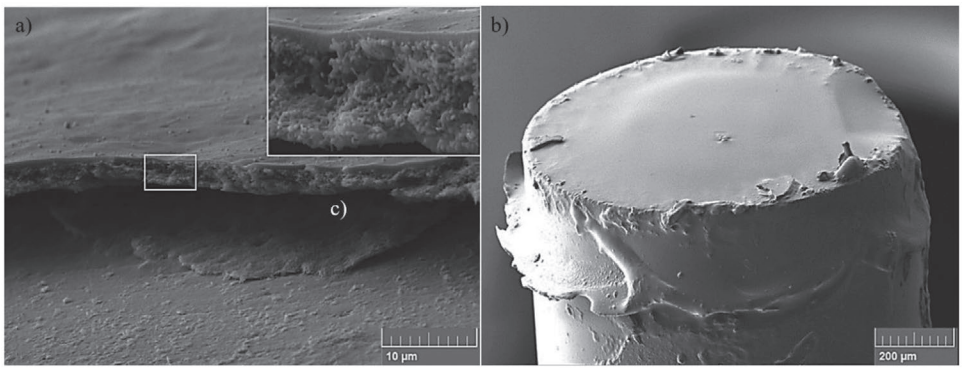

Figure 3. Homogeneity analysis of the layers. a) An uncured CNT-PDMS layer directly after printing shows a high homogeneous distribution without any lumps. b) A subsequently applied PDMS layer with curing agent showing a homogeneous cured structure (after 150 °C for 10 min in the oven). The impurities in (b) come from the manufacturing process, which was not carried out in a specific clean room.

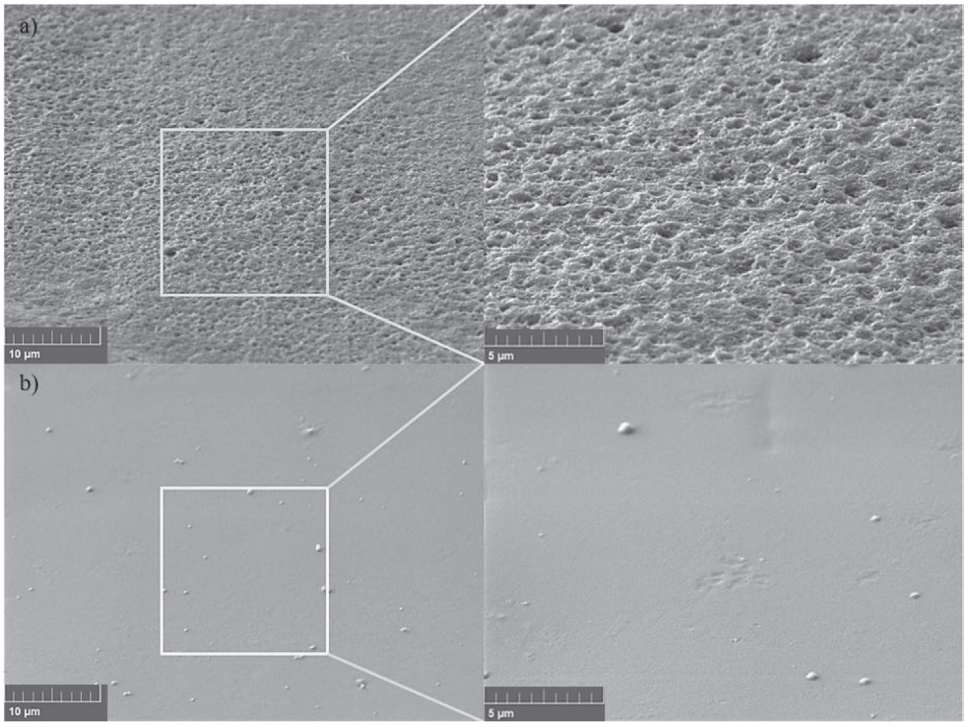

Figure 4. a) Thickness examination of the layers in the SEM imaging. c) Mechanical scraping resulted in all cases a gap between glass fiber and layer. The total thickness of layers is in the range of 2–4 µm. b) Fully inkjet-printed fiber end face after curing.

(12.7 mJ cm^{-2}) for the 1 mm multimode fiber. A digital oscilloscope was applied for data acquisition and signal processing. The distance between the coated fiber end and the hydrophone was ≈4 mm. The measured ultrasound pressures in this setup ranged from 0.39 to 0.54 MPa (**Figure 6**). The corresponding power spectra are shown in Figure 6, with maximum pressure referenced to 0 dB range from 1.5 to 12.7 MHz at a full width of quarter maximum (FWQM) bandwidth.

The signal characteristics of the three fibers are very similar, which indicates that the printing process method has a high reproducibility.

To demonstrate the applicability in medical imaging applications, a silicone dummy sample was prepared, which can be used as cartilage replacement.[75] Silicone was poured into a petri dish and was placed at a slight angle to create a thickness gradient, and it was cured for 48 h. The layer structure of the silicone dummy sample was then scanned with the measurement setup by using a 2D scanning device (**Figure 7**) in the reflection mode.

The measured signals and positions of the scanning device were collected and evaluated with a Matlab program. B-scans or C-scans (**Figure 8**) are reconstructed in the post data processing.

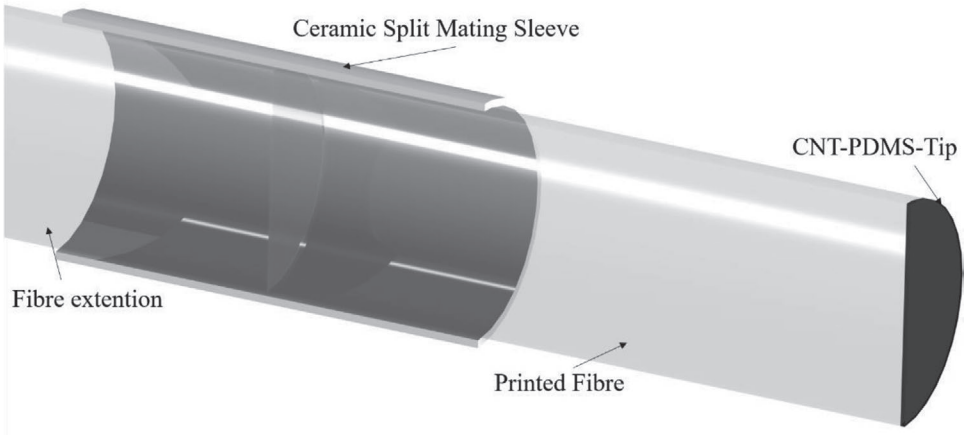

Figure 5. Cross section of fiber assembling shows the method of assembling the short, coated fiber and fiber extension. A mating sleeve was used for alignment and a shrink tube for fastening.

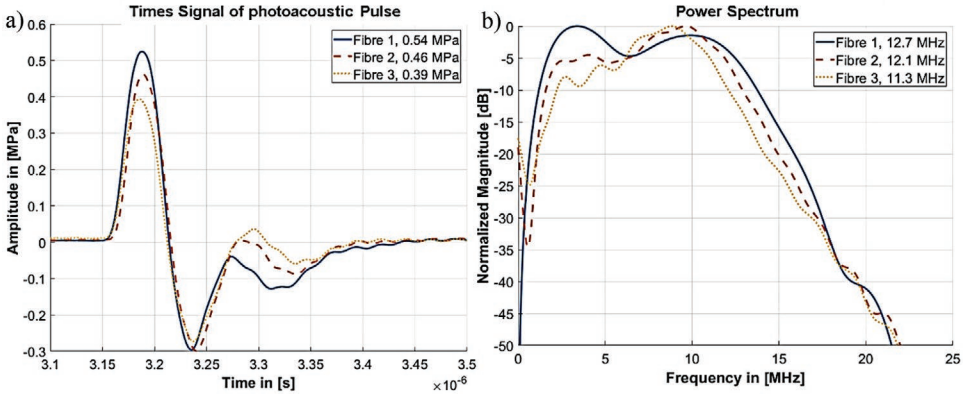

Figure 6. The measured ultrasound pressure pulses of three fully inkjet-printed fiber ultrasonic generators, the ultrasonic pressure amplitudes range from 0.39 to 0.54 MPa measured at ≈4 mm from the distal end of the coated fiber tip. b) The corresponding ultrasonic power spectra range from 1.5 to 12.7 MHz.

4. Conclusion

This study shows successfully the principle of the first reported inkjet-printed photoacoustic generators based on MWCNTs and PDMS. The self-developed inks showed a high long-term stability and thus durability as well as a high printability, which play an important role for the producibility of the thin printed structures and can be prepared under 2 h. The printing process

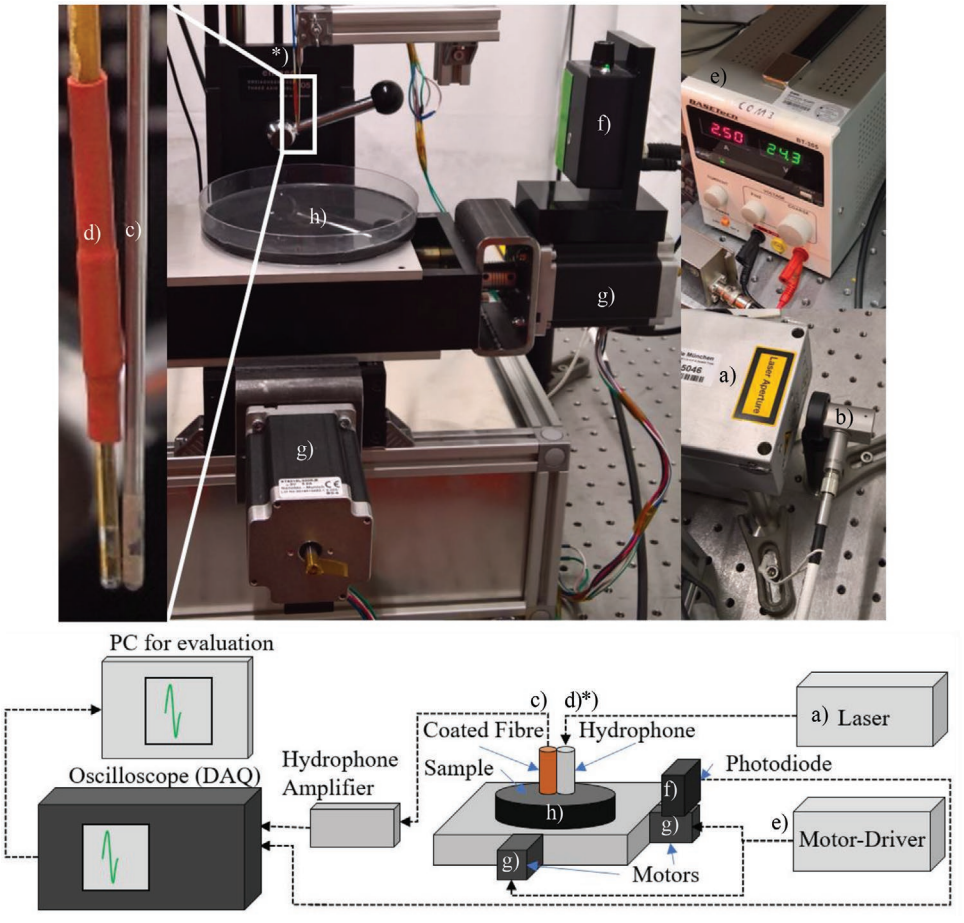

Figure 7. The scanning system for ultrasonic imaging. a) The pulse laser source, b) coupling device for the multimode fiber and the coated fiber*, c) the PVDF needle hydrophone, and d) the coated fiber tip, e) the power supply for the scanning device: g) motors, and f) photodiode for signal triggering. h) Dummy silicone sample.

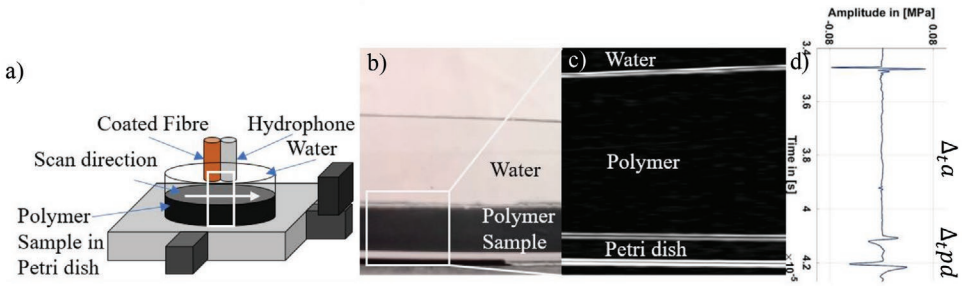

Figure 8. a) Schematic representation of the scanning process for imaging. b) Side view of the silicone sample with a petri dish, ($\Delta_t a$: time of flight in the silicone sample) (see Figure 7). c) The measured B-scan of the silicone disk. B-scan showing the increasing thickness of the polymer and the constant thickness of the petri dish bottom ($\Delta_t pd$: time of flight in the petry dish), and d) a corresponding time signal of a single measurement.

itself can be carried out in a short time (15–20 min). The photoacoustic generator can be produced in less than 3 h from the synthesis of the inks to the printing, curing, and assembling of the fibre. The developed printing inks are well suited for printing, handling, and for industrial printing applications. The printed CNT-PDMS layers on the fibre end faces have a thickness of 2–4 µm and can be used well for high-frequency ultrasonic actuators based on absorption of short laser pulses. The measured ultrasonic pressures ranged from 0.39 to 0.54 MPa at a frequency of 1.5 to 12.7 MHz. The ultrasound pressure generated by an infrared pulse laser source (wavelength of 1047 nm, 11.4 ns pulse duration, and a fluency of 12.7 mJ cm^{-2}) was measured with a PVDF needle hydrophone, which was placed in an ≈4 mm distance of the fibre tips. This novel method of manufacturing thin (2–4 µm) photoacoustic generators based on MWCNT and PDMS offers new possibilities for ultrasound applications in nondestructive materials testing and in medical imaging. The shape and number of layers of the fully inkjet-printed layers can be controlled, which results in a reduction of production time, less costs, and reduced waste for thin layers. Furthermore, the self-developed inks described here offer the possibility to be stored over a long period of time (more than half a year) without changing their printing properties, which is very interesting not only for laboratory environments but also for industrial productions.

Acknowledgements

The authors thank Prof. H. Huber for the use of the laser and the research field "Micro-and Nano-Devices" of the Munich University of Applied Sciences.

Open access funding enabled and organized by Projekt DEAL.

Conflict of Interest

The authors declare no conflict of interest.

Keywords

coatings, inkjet-printing, nanocomposites, nanoparticles, photoacoustics, polymers, thin films

Received: September 4, 2020
Revised: October 19, 2020
Published online: November 16, 2020

[1] E. J. Alles, S. Noimark, E. Maneas, E. Z. Zhang, I. P. Parkin, P. C. Beard, A. E. Desjardins, *Biomed. Opt. Express* **2018**, *9*, 3481.
[2] R. J. Colchester, C. Little, G. Dwyer, S. Noimark, E. J. Alles, E. Z. Zhang, C. D. Loder, I. P. Parkin, I. Papakonstantinou, P. C. Beard, M. C. Finlay, R. D. Rakhit, A. E. Desjardins, *Sci. Rep.* **2019**, *9*, 5576.
[3] Y. Hou, S. Ashkenazi, S.-W. Huang, M. O'Donnell, *IEEE Trans. Ultrason., Ferroelectr., Freq. Control* **2008**, *55*, 2719.
[4] J. Kim, H. Kim, W.-Y. Chang, W. Huang, X. Jiang, P. A. Dayton, *IEEE Nanotechnol. Mag.* **2019**, *13*, 13.
[5] T. Lee, L. J. Guo, *Adv. Opt. Mater.* **2017**, *5*, 1600421.
[6] S.-Y. Hung, W.-S. Wu, B.-Y. Hsieh, P.-C. Li, *J. Biomed. Opt.* **2015**, *20*, 1.
[7] E. J. Alles, S. Noimark, E. Zhang, P. C. Beard, A. E. Desjardins, *Biomed. Opt. Express* **2016**, *7*, 3696.
[8] J. Di, J. Kim, Q. Hu, X. Jiang, Z. Gu, *J. Controlled Release* **2015**, *220*, 592.
[9] E. J. Alles, N. F. Sheung, S. Noimark, E. Z. Zhang, P. C. Beard, A. E. Desjardins, *Sci. Rep.* **2017**, *7*, 1208.
[10] M. C. Finlay, C. A. Mosse, R. J. Colchester, S. Noimark, E. Z. Zhang, S. Ourselin, P. C. Beard, R. J. Schilling, I. P. Parkin, I. Papakonstantinou, A. E. Desjardins, *Light: Sci. Appl.* **2017**, *6*, e17103.
[11] S. Noimark, R. J. Colchester, R. K. Poduval, E. Maneas, E. J. Alles, T. Zhao, E. Z. Zhang, M. Ashworth, E. Tsolaki, A. H. Chester, N. Latif, S. Bertazzo, A. L. David, S. Ourselin, P. C. Beard, I. P. Parkin, I. Papakonstantinou, A. E. Desjardins, *Adv. Funct. Mater.* **2018**, *28*, 1704919.
[12] E. Biagi, F. Margheri, D. Menichelli, *IEEE Trans. Ultrason., Ferroelectr. Freq. Control* **2001**, *48*, 1669.
[13] H. W. Baac, T. Ling, S. Ashkenazi, S.-W. Huang, L. J. Guo, *Proc. SPIE* **2010**, *7564*, 75642M.
[14] M.-A. Park, S. H. Lee, J. J. Yoh, *Appl. Phys. B* **2013**, *113*, 389.
[15] V. V. Kozhushko, P. Hess, *Appl. Phys. Lett.* **2007**, *91*, 224107.
[16] Y. Hou, J.-S. Kim, S. Ashkenazi, S.-W. Huang, L. J. Guo, M. O'Donnell, *Appl. Phys. Lett.* **2007**, *91*, 73507.
[17] Y. Tian, N. Wu, X. Zou, H. Felemban, C. Cao, X. Wang, *Opt. Eng.* **2013**, *52*, 65005.
[18] T. Buma, M. Spisar, M. O'Donnell, *IEEE Trans. Ultrason., Ferroelectr. Freq. Control* **2003**, *50*, 1161.
[19] R. J. Colchester, C. A. Mosse, D. S. Bhachu, J. C. Bear, C. J. Carmalt, I. P. Parkin, B. E. Treeby, I. Papakonstantinou, A. E. Desjardins, *Appl. Phys. Lett.* **2014**, *104*, 173502.

[20] N. Wu, Y. Tian, X. Zou, X. Wang, *Proc. SPIE* **2013**, *8694*, 86940Q.
[21] X. Zou, N. Wu, Y. Tian, X. Wang, *Opt. Express* **2014**, *22*, 18119.
[22] E. J. Alles, S. Noimark, E. Maneas, E. Z. Zhang, I. P. Parkin, P. C. Beard, A. E. Desjardins, *Biomed. Opt. Express* **2018**, *9*, 3481.
[23] E. Biagi, F. Margheri, D. Menichelli, *IEEE Trans. Ultrason., Ferroelectr. Freq. Control* **2001**, *48*, 1669.
[24] B.-Y. Hsieh, J. Kim, J. Zhu, S. Li, X. Zhang, X. Jiang, *Appl. Phys. Lett.* **2015**, *106*, 21902.
[25] W.-Y. Chang, W. Huang, J. Kim, S. Li, X. Jiang, *Appl. Phys. Lett.* **2015**, *107*, 161903.
[26] Y. Hou, S. Ashkenazi, S.-W. Huang, M. O'Donnell, *IEEE Trans. Ultrason., Ferroelectr. Freq. Control* **2007**, *54*, 682.
[27] Y. Li, Z. Guo, G. Li, S.-L. Chen, *Opt. Express.* **2018**, *26*, 21700.
[28] W.-Y. Chang, X. A. Zhang, J. Kim, W. Huang, A. Bagal, C.-H. Chang, T. Fang, H. F. Wu, X. Jiang, *IEEE Trans. Nanotechnol.* **2018**, *17*, 985.
[29] M. Faraz, M. A. Abbasi, P. Sang, D. Son, H. W. Baac, *Micromachines* **2020**, *11*, 631.
[30] H. W. Baac, J. G. Ok, H. J. Park, T. Ling, S.-L. Chen, A. J. Hart, L. J. Guo, *Appl. Phys. Lett.* **2010**, *97*, 234104.
[31] H. W. Baac, J. G. Ok, T. Lee, L. J. Guo, *Nanoscale* **2015**, *7*, 14460.
[32] K. Mizunoa, J. Ishiib, H. Kishidac, Y. Hayamizua, S. Yasudaa, D. N. Futabaa, M. Yumuraa, K. Hataa, *Proc. Natl. Acad. Sci. USA* **2009**, *106*, 6044.
[33] X. J. Wang, J. D. Flicker, B. J. Lee, W. J. Ready, Z. M. Zhang, *Nanotechnology* **2009**, *20*, 215704.
[34] T. de los Acros, P. Oelhafen, D. Mathys, *Nanotechnology* **2007**, *18*, 265706.
[35] K. Cui, B. L. Wardle, *ACS Appl. Mater. Interfaces* **2019**, *11*, 35212.
[36] N. Bowden, W. T. S. Huck, K. E. Paul, G. M. Whitesides, *Appl. Phys. Lett.* **1999**, *75*, 2557.
[37] C. Moon, X. Fan, K. Ha, D. Kim, *AIP Adv.* **2017**, *7*, 15107.
[38] H. W. Baac, J. G. Ok, A. Maxwell, K.-T. Lee, Y.-C. Chen, A. J. Hart, Z. Xu, E. Yoon, L. J. Guo, *Sci. Rep.* **2012**, *2*, 989.
[39] D. K. Cai, A. Neyer, R. Kuckuk, H. M. Heise, *Opt. Mater.* **2008**, *30*, 1157.
[40] N. E. Stankova, P. A. Atanasov, R. G. Nikov, R. G. Nikov, N. N. Nedyalkov, T. R. Stoyanchov, N. Fukata, K. N. Kolev, E. I. Valova, J. S. Georgieva, St. A. Armyanov, *Appl. Surf. Sci.* **2016**, *374*, 96.
[41] P. Oser, O. Düttmann, F. Schmid, L. Schulte-Spechtel, C. U. Große, D. Wu, *Macromol. Mater. Eng.* **2020**, *305*, 1900852.
[42] R. J. Colchester, C. A. Mosse, D. I. Nikitichev, E. Z. Zhang, S. West, P. C. Beard, I. Papakonstantinou, A. E. Desjardins, *Photon Plus Ultrasound: Imaging Sens.* **2015**, *9323*, 932321.
[43] T. Lee, J. G. Ok, L. J. Guo, H. W. Baac, *Appl. Phys. Lett.* **2016**, *108*, 104102.
[44] S. Noimark, R. J. Colchester, B. J. Blackburn, E. Z. Zhang, E. J. Alles, S. Ourselin, P. C. Beard, I. Papakonstantinou, I. P. Parkin, A. E. Desjardins, *Adv. Funct. Mater.* **2016**, *26*, 8390.
[45] R. K. Poduval, S. Noimark, R. J. Colchester, T. J. Macdonald, I. P. Parkin, A. E. Desjardins, I. Papakonstantinou, *Appl. Phys. Lett.* **2017**, *110*, 223701.
[46] X. Fan, Y. Baek, K. Ha, M. Kim, J. Kim, D. Kim, H. W. Kang, J. Oh, *Jpn. J. Appl. Phys.* **2017**, *56*, 07JB05.
[47] X. Fan, K. Ha, M. Kim, G. Kang, M. J. Choi, J. Oh, *Jpn. J. Appl. Phys.* **2018**, *57*, 07LB10.
[48] S. K. Eshkalak, A. Chinnappan, W. A. D. M. Jayathilaka, M. Khatibzadeh, E. Kowsari, S. Ramakrishna, *Appl. Mater. Today* **2017**, *9*, 372.
[49] K. Kordás, T. Mustonen, G. Tóth, H. Jantunen, M. Lajunen, C. Soldano, S. Talapatra, S. Kar, R. Vajtai, P. M. Ajayan, *Small* **2006**, *2*, 1021.
[50] A. Shimoni, S. Azoubel, S. Magdassi, *Nanoscale* **2014**, *6*, 11084.
[51] R. P. Tortorich, J.-W. Choi, *Nanomaterials* **2013**, *3*, 453.
[52] T. Wei, J. Ruan, Z. Fan, G. Luo, F. Wei, *Carbon* **2007**, *45*, 2712.
[53] Y. J. Zhao, C. Beisteiner, S. Gschossmann, M. Schagerl, *Adv. Sci. Technol.* **2016**, *101*, 3.
[54] W. Honda, S. Harada, T. Arie, S. Akita, K. Takei, *presented at SENSORS, 2014 IEEE, Valencia*, Spain, November **2014**.
[55] C. Gerlach, J. Lange, O. Kanoun, presented at 2012 IEEE 9th Int. Multi-Conf. Systems, Signals and Devices (SSD), Chemnitz, Germany, March **2012**.
[56] J. H. Kim, J.-Y. Hwang, H. R. Hwang, H. S. Kim, J. H. Lee, J.-W. Seo, U. S. Shin, S.-H. Lee, *Sci. Rep.* **2018**, *8*, 1375.
[57] N. Yogeswaran, S. Tinku, S. Khan, L. Lorenzelli, V. Vinciguerra, R. Dahiya, presented at 2015 11th Conf. Ph.D. Research in Microelectronics and Electronics (PRIME), Glasgow, UK, June **2015**.
[58] S. Pyo, J.-I. Lee, M.-O. Kim, T. Chung, Y. Oh, S.-C. Lim, J. Park, J. Kim, *J. Micromech. Microeng.* **2014**, *24*, 75012.
[59] L. Wu, J. Qian, J. Peng, K. Wang, Z. Liu, T. Ma, Y. Zhou, G. Wang, S. Ye, *J. Mater. Sci.: Mater. Electron.* **2019**, *30*, 9593.
[60] C. S. O'Bryan, T. Bhattacharjee, S. Hart, C. P. Kabb, K. D. Schulze, I. Chilakala, B. S. Sumerlin, W. G. Sawyer, T. E. Angelini, *Am. Assoc. Adv. Sci.* **2017**, *3*, 1.
[61] T. J. Hinton, A. Hudson, K. Pusch, A. Lee, A. W. Feinberg, *ACS Biomater. Sci. Eng.* **2016**, *2*, 1781.
[62] S. Harada, W. Honda, T. Arie, S. Akita, K. Takei, *ACS Nano.* **2014**, *8*, 3921.
[63] K. S. Karimov, M. T. S. Chani, F. A. Khalid, *Phys. E* **2011**, *43*, 1701.
[64] K. H. S. Karimov, F. A. Khalid, M. T. S. Chani, A. Mateen, M. A. Hussain, A. Maqbool, *Optoelectron. Adv. Mater., Rapid Commun.* **2012**, *6*, 194.
[65] A. S. Kurian, T. Giffney, J. Lee, J. Travas-Sejdic, K. C. Aw, presented at *SPIE Smart Structures and Materials + Nondestructive Evaluation and Health Monitoring*, Las Vegas, NV, March **2016**.
[66] Y. Zhao, M. Schageri, presented at 8th European Workshop on Structural Health Monitoring (EWSHM 2016), Bilbao, Spain, July **2016**.
[67] H. Wang, W. Zhou, D. L. Ho, K. I. Winey, J. E. Fischer, C. J. Glinka, E. K. Hobbie, *Nano Lett.* **2004**, *4*, 1789.
[68] Y. Geng, M. Y. Liu, J. Li, X. M. Shi, J. K. Kim, *Composites, Part A* **2008**, *39*, 1876.
[69] Y. Bai, D. Lin, F. Wu, Z. Wang, B. Xing, *Chemosphere* **2010**, *79*, 362.
[70] R. Rastogi, R. Kaushal, S. K. Tripathi, A. L. Sharma, I. Kaur, L. M. Bharadwaj, *J. Colloid Interface Sci.* **2008**, *328*, 421.
[71] L. Vaisman, G. Marom, H. D. Wagner, *Adv. Funct. Mater.* **2006**, *16*, 357.
[72] J. N. Lee, C. Park, G. M. Whitesides, *Anal. Chem.* **2003**, *75*, 6544.
[73] A. Mamidanna, C. Lefky, O. Hildreth, *Microfluid. Nanofluid.* **2017**, *21*, R15.
[74] R. Mikkonen, P. Puistola, I. Jönkkäri, M. Mäntysalo, *ACS Appl. Mater. Interfaces* **2020**, *12*, 11990.
[75] J.-Y. Hong, S. Yun, J. J. Wie, X. Zhang, M. S. Dresselhaus, J. Kong, H. S. Park, *Nanoscale* **2016**, *8*, 12900.